

# Persistent Skyrmion Lattice of Non-Interacting Electrons in Spin-Orbit Coupled Double Wells

Jiyong Fu,<sup>1,\*</sup> Poliana H. Penteado,<sup>1</sup> Marco O. Hachiya,<sup>1</sup> Daniel Loss,<sup>2</sup> and J. Carlos Egues<sup>1</sup>

<sup>1</sup>*Instituto de Física de São Carlos, Universidade de São Paulo, 13560-970, São Carlos, São Paulo, Brazil*

<sup>2</sup>*Department of Physics, University of Basel, CH-4056 Basel, Switzerland*

(Dated: September 22, 2018)

A persistent spin helix (PSH) is a robust helical spin-density pattern arising in disordered 2D electron gases with Rashba  $\alpha$  and Dresselhaus  $\beta$  spin-orbit (SO) tuned couplings, i.e.,  $\alpha = \pm\beta$ . Here we investigate the emergence of a Persistent Skyrmion Lattice (PSL) resulting from the coherent superposition of PSHs along orthogonal directions – crossed PSHs – in wells with two occupied subbands  $\nu = 1, 2$ . Our calculation shows that the Rashba  $\alpha_\nu$  and Dresselhaus  $\beta_\nu$  couplings can be simultaneously tuned to equal strengths but opposite signs, e.g.,  $\alpha_1 = \beta_1$  and  $\alpha_2 = -\beta_2$ . In this regime and away from band anticrossings, our non-interacting electron gas sustains a topologically non-trivial skyrmion-lattice spin-density excitation, which inherits the robustness against time-reversal conserving perturbations from its underlying crossed PSHs. We find that the spin relaxation rate due to the interband SO coupling is comparable to that of the cubic Dresselhaus term as a mechanism for the PSL decay. Near the anticrossing, the strong interband-induced spin mixing leads to unusual spin textures along the energy contours beyond those of the Rashba-Dresselhaus bands. We consider realistic GaAs and InSb wells for possible experiments.

PACS numbers: 71.70.Ej, 75.70.Tj, 72.25.Rb

**Introduction.** — Recently spin-orbit (SO) effects have attracted renewed interest due to: (i) the discovery of topological insulators [1–4], in which the SO interaction inextricably locks spin and momentum in their gapless helical edge (or surface) states and (ii) the possibility of detecting Majorana modes in superconducting SO-coupled nanowires [5].

Unconventional spin textures in electron systems are usually due to the electron-electron interaction, e.g., skyrmions in the fractional quantum Hall regime [6, 7], magnetic and multiferroic systems [8], and spin-density waves in metals [9]. Non-interacting electrons can sustain unusual spin textures only in the presence of the SO interaction. A remarkable example is the persistent spin helix (PSH) [10, 11], a spin-density wave excitation robust against any time-reversal conserving interaction, occurring in 2D electron gases when the Rashba and Dresselhaus SO interactions are tuned equal ( $\alpha = \pm\beta$ ). This symmetry point uniquely defines a direction along which a spin component is conserved [10]. Koralek *et al.* first observed a PSH via transient spin grating spectroscopy [12]; Walser *et al.* imaged PSHs using time-resolved Kerr rotation microscopy [13]. See Ref. [14] for further experimental work.

Here we study the emergence of PSH excitations along orthogonal directions — crossed PSHs — in double-well structures with two occupied subbands [15, 16] and SO couplings of opposite signs (Rashba Fig. 1). Our energy dispersions feature two Dirac cones at  $\mathbf{k} = 0$  Fig. 1(a) and anticrossings with strong spin mixing [significant in InSb, Fig. 2(a)] and highly anisotropic four-branch Fermi contours. Interestingly, away from the anticrossings we find a non-trivial skyrmionic spin texture, which we refer to as Persistent Skyrmion Lattice (PSL) Fig. 1(e), arising from the coherent superposition of orthogonal PSHs. The PSL here is topologically identical to the ‘spin crystal’ in Ref. [17].

More specifically, our self-consistent Hartree calculation for realistic GaAs double wells shows the feasibility of tuning

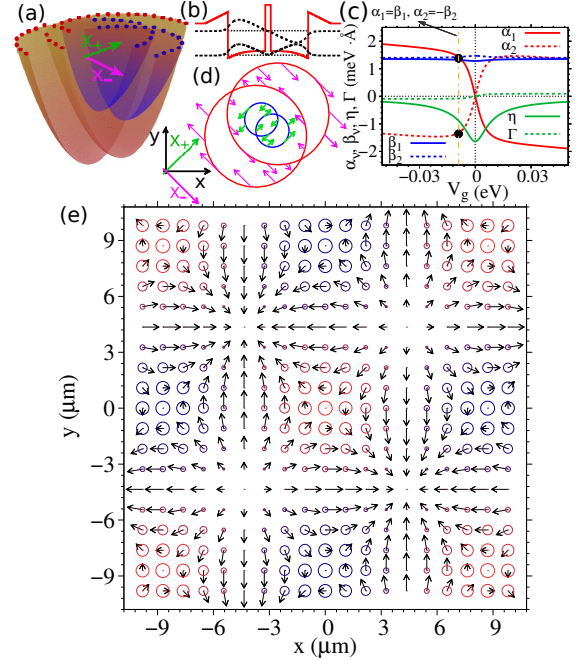


Figure 1. (Color online) (a) Energy dispersion for a realistic GaAs double well with two subbands. (b) Schematic profile of the potential and wave functions. (c) Self-consistent calculated SO couplings vs.  $V_g$ : intraband (interband) Rashba  $\alpha_\nu$  ( $\eta$ ) and Dresselhaus  $\beta_\nu$  ( $\Gamma$ ). The dot-dashed vertical line (orange) indicates the crossed PSH symmetry point  $\alpha_1 = \beta_1$  and  $\alpha_2 = -\beta_2$ . (d) Energy contours; the arrows pointing along the orthogonal axes  $x_-$  (pink) and  $x_+$  (green) define the subband SO fields  $B_1^{SO}$  and  $B_2^{SO}$ , respectively. (e) Persistent Skyrmion Lattice (PSL) pattern in the 2DEG. The size of the circles and arrows denote  $\langle s_z \rangle$  and  $\langle s_{x,y} \rangle$ , respectively. Blue (dark gray) circles stand for spins up and red (light gray) for spins down.

the strengths of the Rashba  $\alpha_\nu$  and Dresselhaus  $\beta_\nu$  couplings within each subband  $\nu = 1, 2$ , such that  $\alpha_1 = \beta_1$  and  $\alpha_2 = -\beta_2$

[see dot-dashed vertical line in Fig. 1(c)]. At this symmetry point, our 2DEG has two preferential orthogonal axes ( $\hat{x}_-, \hat{x}_+$ ), Fig. 1(d), along which two distinct spin components are conserved, one for each subband. Hence crossed PSHs emerge, which leads to a robust persistent skyrmion lattice pattern. We derive analytical expressions for the PSL in Fig. 1(e) quantum mechanically including disorder [10] and from diffusive equations for the coupled spin and charge densities [11, 18, 19].

*Model Hamiltonian.*— We consider electrons confined in a quantum well with the SO interactions of the Rashba and Dresselhaus types. We start with the 3D Hamiltonian [20]

$$H = H_{\text{QW}} + \frac{\eta}{\hbar} (\sigma_y p_x - \sigma_x p_y) + \frac{\gamma}{\hbar} [p_x (p_y^2 - p_z^2) \sigma_x + \text{c.p.}], \quad (1)$$

where  $\sigma_{x,y,z}$  are the spin Pauli matrices,  $p_{x,y,z}$  the electron momentum components along the  $x \parallel [100]$ ,  $y \parallel [010]$ ,  $z \parallel [001]$  directions,  $m^*$  the effective electron mass, and  $H_{\text{QW}} = (p_x^2 + p_y^2)/2m^* + p_z^2/2m^* + V_{\text{sc}}(z)$ . Here  $V_{\text{sc}}$  denotes the “self consistent” potential felt by the confined electrons. It comprises the structural part  $V_w$ , the electronic Hartree potential  $V_e$ , the doping potential  $V_d$  and an external gate  $V_g$ . The coefficient  $\gamma$  (assumed constant) is the bulk Dresselhaus parameter [21] and  $\eta(z) = \eta_w \partial_z V_w + \eta_H \partial_z (V_e + V_g + V_d)$  defines the strength of the Rashba coupling [22]. The parameters  $\eta_w$  and  $\eta_H$  contain bulk quantities of the well layer.

We now derive an effective 2D Hamiltonian by projecting  $H$  in Eq. (1) onto the *two* lowest spin-degenerate plane-wave eigensolutions of  $H_{\text{QW}}$ :  $\langle \mathbf{r} | \mathbf{k}, \nu, \sigma \rangle = e^{i\mathbf{k}\cdot\mathbf{r}} \varphi_\nu(z) |\sigma_z\rangle$ ,  $\nu = 1, 2, \dots$ ,  $\sigma_z = \uparrow, \downarrow$ , with energies  $\varepsilon_{\nu,k} = \varepsilon_\nu + \hbar^2 k^2 / 2m^*$ , where  $\mathbf{k}$  is the in-plane electron wave vector and  $\varepsilon_\nu$  is the  $\nu$ th confined well level in the absence of SO. Choosing  $x \rightarrow x_+ \parallel [110]$ ,  $y \rightarrow x_- \parallel [1\bar{1}0]$ , we find the  $4 \times 4$  Hamiltonian

$$\mathcal{H} = \left( \frac{\hbar^2 k^2}{2m^*} + \varepsilon_\pm \right) \mathbb{1} \otimes \mathbb{1} - \varepsilon_- \tau_z \otimes \mathbb{1} + \mathcal{H}_{\text{RD}}, \quad (2)$$

in which  $\varepsilon_\pm = (\varepsilon_2 \pm \varepsilon_1)/2$ ,  $\tau_j$  ( $j = x_+, x_-, z$ ) the Pauli matrices in the subband subspace, and

$$\mathcal{H}_{\text{RD}} = \frac{g^* \mu_B}{2} [ \mathbb{1} \otimes \sigma \cdot \mathbf{B}_+^{SO}(\mathbf{k}) - \tau_z \otimes \sigma \cdot \mathbf{B}_-^{SO}(\mathbf{k}) + \tau_{x_+} \otimes \sigma \cdot \mathbf{B}_{12}^{SO}(\mathbf{k}) ], \quad (3)$$

with  $g^*$  the effective g-factor,  $\mu_B$  the Bohr magneton,  $\mathbf{B}_\pm^{SO} = (\mathbf{B}_2^{SO} \pm \mathbf{B}_1^{SO})/2$ , and  $\sigma_j$  the Pauli matrices in the spin subspace.

We can write the intraband  $\mathbf{B}_\nu^{SO}(\mathbf{k})$  effective magnetic field in terms of the 1st and 3rd harmonics ( $\sin/\cos$  of  $\theta$  and  $3\theta$ ) [23]

$$\mathbf{B}_\nu^{SO} = \frac{2k}{g^* \mu_B} \left\{ [(\alpha_\nu - \beta_\nu) \sin \theta - \beta_{3,\nu} \sin 3\theta] \hat{\mathbf{x}}_+ - [(\alpha_\nu + \beta_\nu) \cos \theta - \beta_{3,\nu} \cos 3\theta] \hat{\mathbf{x}}_- \right\}, \quad (4)$$

with  $\tan \theta = (k_{x_+}/k_{x_-})$  and the *intraband* SO couplings  $\alpha_\nu = \langle \nu | \eta(z) | \nu \rangle$  (Rashba) and  $\beta_\nu = \beta_{1,\nu} - \beta_{3,\nu}$  (Dresselhaus);  $\beta_{1,\nu} = \gamma \langle \nu | k_z^2 | \nu \rangle$  and  $\beta_{3,\nu} = \gamma k^2 / 4$  (cubic Dresselhaus). At the Fermi energy  $\beta_{3,\nu} \approx \gamma \pi n_\nu / 2$ , where we used  $k_{F,\nu} \approx \sqrt{2\pi n_\nu}$  as the Fermi wave vector for the  $\nu$ th subband ( $k_{F,1} \approx k_{F,2}$  here), with

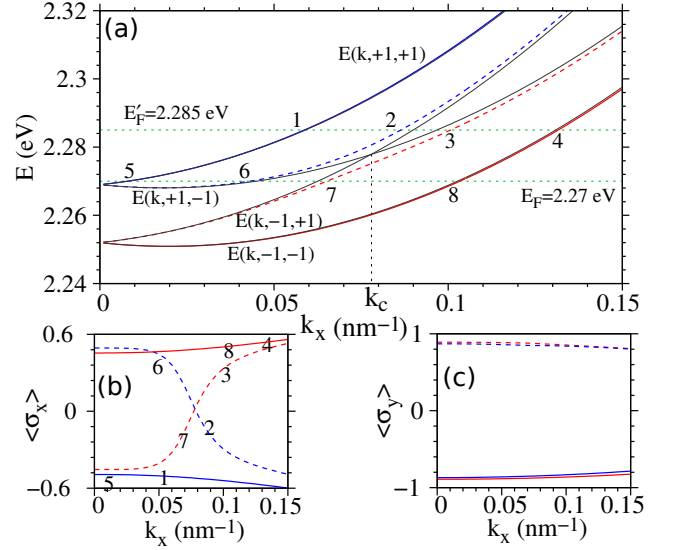


Figure 2. (Color online) (a) Energy dispersions  $E_{k,+1,\pm 2}$  (scaled by a factor of 10) along the  $k_{x_+} = k_{x_-}$  direction for an InSb double well. The black solid lines correspond to the uncoupled ( $\eta = \Gamma = 0$ ) Rashba-Dresselhaus subbands  $E_{\nu,k}^\pm$  and cross at  $k_c$  [35]. For  $\eta, \Gamma \neq 0$  these bands anticross (dashed lines). Away from  $k_c$ , the coupled and uncoupled cases coincide. The label sets (1, 2, 3, 4) and (5, 6, 7, 8) denote Fermi points along  $k_{x_+} = k_{x_-}$  at  $E'_F$  and  $E_F$ , respectively. Panels (b) and (c) show the expectation values of the spin operators  $\sigma_x$  and  $\sigma_y$ , respectively, as functions of  $k_x$ . The solid and dashed lines correspond to the respective energy branches in (a).

areal electron density  $n_\nu$ . Note that  $\beta_{3,\nu}$  renormalizes the linear Dresselhaus coupling  $\beta_{1,\nu}$  and leads to the PSH condition  $\alpha_\nu = \pm \beta_\nu$  (not  $\alpha_\nu = \pm \beta_{1,\nu}$ ). The interband SO field

$$\mathbf{B}_{12}^{SO} = \frac{2k}{g^* \mu_B} [(\eta - \Gamma) \sin \theta \hat{\mathbf{x}}_+ - (\eta + \Gamma) \cos \theta \hat{\mathbf{x}}_-] \quad (5)$$

contains only the 1st harmonic. Here  $\eta = \langle \nu | \eta(z) | \nu' \rangle$  and  $\Gamma = \gamma \langle \nu | k_z^2 | \nu' \rangle$  denote the Rashba and Dresselhaus *interband* SO couplings [24], respectively.

*Self consistent SO couplings for a GaAs double well.*— We consider two 210 Å wells of depth  $V_w = 261$  meV and separated by a 30 Å barrier of height  $V_b = V_w$  Fig. 1(b). The electron density  $n = 4.8 \times 10^{11} \text{ cm}^{-2}$  (spanning two subbands with  $n_1 = 2.48$  and  $n_2 = 2.32 \times 10^{11} \text{ cm}^{-2}$ ) is due to modulation doping layers symmetrically placed 345 Å away from the center of the double well. We solve both Schrödinger and Poisson’s equations to obtain the self-consistent eigenfunctions  $\varphi_\nu(z)$ , which we then use to calculate the relevant SO couplings. In Fig. 1(c), we show the intraband (interband) Rashba  $\alpha_\nu$  ( $\eta$ ) and Dresselhaus  $\beta_\nu$  ( $\Gamma$ ) couplings as functions of  $V_g$ . We observe that  $\alpha_1$  and  $\alpha_2$  are very sensitive to the gate voltage and, more importantly, have opposite signs. On the other hand,  $\beta_1$  and  $\beta_2$  ( $\beta_1 \approx \beta_2$ ) are practically independent of  $V_g$  [15]. At the symmetry point,  $V_g = 10$  meV (dot-dashed vertical line), we find  $\alpha_1 = \beta_1 = -\alpha_2 = \beta_2 = 1.45 \text{ meV \AA}$  (black dots),  $\eta = -0.8 \text{ meV \AA}$  and  $\Gamma = -0.08 \text{ meV \AA}$ .

*Robust eigensolutions at the symmetry point.* — The 3rd harmonic cubic Dresselhaus (spin relaxation) and the interband SO couplings (anticrossing, spin mixing, spin relaxation) can be negligible, e.g., in GaAs wells, Fig. 1, where  $E_F$  lies in the 2nd subband but far below band crossings. In this case and including an arbitrary non-magnetic potential  $V(\mathbf{r})$ , due to, e.g., disorder [10],  $\mathcal{H}$  at  $\alpha_1 = \beta_1$  and  $\alpha_2 = -\beta_2$  becomes  $\tilde{\mathcal{H}} = \mathcal{H} + V(\mathbf{r})$ . Here  $\mathcal{H}$  neglects the 3rd harmonic and interband SO terms.

Interestingly, for an arbitrary non-magnetic  $V(\mathbf{r})$ ,  $\tilde{\mathcal{H}}$  admits eigensolutions of the form  $\psi_1^{\uparrow x_-}(\mathbf{r}) = \varphi(\mathbf{r})e^{iQ_1 x_+ / 2} |\uparrow_{x_-}\rangle$  and  $\psi_1^{\downarrow x_-}(\mathbf{r}) = \varphi(\mathbf{r})e^{-iQ_1 x_+ / 2} |\downarrow_{x_-}\rangle$  for subband 1 and similarly  $\psi_2^{\uparrow x_+}(\mathbf{r}) = \varphi(\mathbf{r})e^{iQ_2 x_- / 2} |\uparrow_{x_+}\rangle$  and  $\psi_2^{\downarrow x_+}(\mathbf{r}) = \varphi(\mathbf{r})e^{-iQ_2 x_- / 2} |\downarrow_{x_+}\rangle$  for subband 2. Here  $Q_\nu = 4m^* \alpha_\nu / \hbar^2$  ( $\nu = 1, 2$ ) and  $|\uparrow_{x_\pm}\rangle, |\downarrow_{x_\pm}\rangle$  are the eigenvectors of the operator  $\sigma_{x_\pm}$ , i.e., states with spin components parallel or antiparallel to the axes  $x_\pm$ . The ‘‘envelope function’’  $\varphi(\mathbf{r})$  satisfies  $(-\hbar^2 \nabla^2 / 2m^* + V(\mathbf{r}))\varphi(\mathbf{r}) = (\varepsilon - \varepsilon_\nu + 2\alpha_\nu^2 m^* / \hbar^2)\varphi(\mathbf{r})$  [25]. The eigensolutions of  $\tilde{\mathcal{H}}$ , ir-respective of the disorder potential, possess (i) spin states that are robust against scattering (the spin and orbital parts are factorized) and (ii) well defined SO-induced spin-rotation phases that only depend on the distance ‘traveled’ along the relevant direction ( $\hat{x}_+$  or  $\hat{x}_-$ ). This is so because  $[\tilde{\mathcal{H}}, \mathbb{1} \otimes \sigma_{x_\pm}] = 0$ .

*Persistent Skyrmion Lattice: Quantum approach* — Let us consider the linear combinations of quantum states  $\psi_1(\mathbf{r}) = \varphi(\mathbf{r})(e^{iQ_1 x_+ / 2} |\uparrow_{x_-}\rangle + e^{-iQ_1 x_+ / 2} |\downarrow_{x_-}\rangle) / \sqrt{2}$  and  $\psi_2(\mathbf{r}) = \varphi(\mathbf{r})(e^{iQ_2 x_- / 2} |\uparrow_{x_+}\rangle + e^{-iQ_2 x_- / 2} |\downarrow_{x_+}\rangle) / \sqrt{2}$  representing stationary spin up states at  $\mathbf{r} = 0$  within each subband. The spin density profile  $\mathbf{s}(\mathbf{r})$  arising from the superposition  $|\mathbf{r}\rangle\langle\psi| = \psi(\mathbf{r}) = \psi_1(\mathbf{r}) + \psi_2(\mathbf{r})$  at a given energy is

$$\begin{aligned} \mathbf{s}(\mathbf{r}) &= \mathbf{s}(x_+, x_-) = \langle\psi|\mathbb{1} \otimes \frac{1}{2}(\sigma_{x_+} \hat{x}_+ + \sigma_{x_-} \hat{x}_- + \sigma_z \hat{z})|\psi\rangle \\ \mathbf{s}(\mathbf{r}) &= \frac{1}{4}|\varphi(\mathbf{r})|^2 \left\{ -\sin(Q_1 x_+) \hat{x}_+ + \sin(Q_2 x_-) \hat{x}_- + \right. \\ &\quad \left. [\cos(Q_1 x_+) + \cos(Q_2 x_-)] \hat{z} \right\}. \end{aligned} \quad (6)$$

Interestingly,  $\mathbf{s}(\mathbf{r})$  forms a ‘persistent skyrmion lattice’ [17], Fig. 1(e) [26], arising from two orthogonal PSHs, along  $\hat{x}_+$  (1st subband) and  $\hat{x}_-$  (2nd subband), respectively. Note that our PSL inherits the robustness from its constituent persistent spin helices. In strict analogy to Ref. [17], we can define  $\hat{\mathbf{n}} = \mathbf{s}/|\mathbf{s}|$  and show that the PSL is characterized by a skyrmion number over the PSL unit cell area  $S$ :  $\frac{1}{4\pi} \int_S \hat{\mathbf{n}} \cdot (\partial_x \hat{\mathbf{n}} \times \partial_y \hat{\mathbf{n}}) dx dy$ .

*Semiclassical approach.* — Following Refs. [11, 18, 27], we solve a set of diffusive transport equations, valid in the limit  $\alpha_\nu k_F \tau \ll 1$ ,  $\beta_\nu k_F \tau \ll 1$  [28–30], with  $\tau$  the momentum scattering time, for the coupled dynamics of spin  $s_{x_\pm, x_\mp, z}^\nu(x_+, x_-, t)$  and charge  $n^\nu(x_+, x_-, t)$  densities in subbands  $\nu = 1, 2$ . At the symmetry point  $\alpha_1 = \beta_1$  and  $\alpha_2 = -\beta_2$ , the Fourier component of  $s_z^1$  obeys

$$\begin{aligned} \partial_t^2 s_z^1(q_{x_+}, q_{x_-}, t) + 2(Dq^2 + T)\partial_t s_z^1(q_{x_+}, q_{x_-}, t) + \\ [(Dq^2 + T)^2 - Cq_{x_+}]s_z^1(q_{x_+}, q_{x_-}, t) = 0, \end{aligned} \quad (7)$$

where  $q^2 = q_{x_+}^2 + q_{x_-}^2$ ,  $D = v_F^2 \tau / 2$  the diffusion constant,  $v_F = \hbar k_F / m^*$  the Fermi velocity,  $C = 4\alpha_1 k_F^2 \tau / m^*$  and  $T =$

$8\alpha_1^2 k_F^2 \tau / \hbar^2$ . The solution to (7) is

$$s_z^1(\mathbf{q}, t) = A_+(\mathbf{q})e^{-\omega_+(\mathbf{q})t} + A_-(\mathbf{q})e^{-\omega_-(\mathbf{q})t} \quad (8)$$

where  $A_\pm(\mathbf{q})$  are amplitudes set by the initial conditions  $[s_z^1(\mathbf{q}, 0)$  and  $\partial_t s_z^1(\mathbf{q}, t)|_{t=0}]$ , and  $\omega_\pm(\mathbf{q}) = Dq^2 + T \pm Cq_{x_+}$ . Equations similar to (7), with distinct initial conditions, hold for  $s_{x_\pm}^1$ , while  $s_{x_-}^1$  obeys  $\partial_t^2 s_{x_-}^1(\mathbf{q}) = Dq^2 s_{x_-}^1(\mathbf{q})$ . At the symmetry point the charge density is also fully decoupled:  $\partial_t^2 n^1(\mathbf{q}) = Dq^2 n^1(\mathbf{q})$ . For the 2nd subband  $s_z^2(q_{x_+}, q_{x_-}, t) = s_z^2(q_{x_-}, q_{x_+}, t)$  and  $s_{x_-}^2(q_{x_+}, q_{x_-}, t) = -s_{x_+}^2(q_{x_-}, q_{x_+}, t)$ . Hence given an arbitrary initial spin density  $\mathbf{s}(\mathbf{q}, t = 0)$  [or equivalently  $\mathbf{s}(\mathbf{r}, t = 0)$ ], we can determine  $s_j(\mathbf{q}, t) = s_j^1(\mathbf{q}, t) + s_j^2(\mathbf{q}, t)$ ,  $j = x_+, x_-, z$  and the spin-density profile  $s_j(\mathbf{r}, t) = \int s_j(\mathbf{q}, t) \exp(i\mathbf{q} \cdot \mathbf{r}) d\mathbf{q}$ . Next we show how a PSL emerges in this description.

*Transient ‘‘crossed’’ spin gratings: induced PSL* — Let us first consider a variant of the transient spin grating experiment of Koralek *et al.* [12], i.e., a setup with crossed lasers  $a$  and  $b$  giving rise to two orthogonal spin gratings with a initial spin density given by  $s_z(\mathbf{r}, 0) = \cos(q_{x_+}^a x_+) + \cos(q_{x_-}^b x_-)$  and  $s_{x_+}(\mathbf{r}, 0) = s_{x_-}(\mathbf{r}, 0) = 0$ . In this case,  $A_+(\mathbf{q}) = A_-(\mathbf{q}) = [\delta(\mathbf{q} + q_{x_+}^a \hat{x}_+) + \delta(\mathbf{q} - q_{x_+}^a \hat{x}_+) + \delta(\mathbf{q} + q_{x_-}^b \hat{x}_-) + \delta(\mathbf{q} - q_{x_-}^b \hat{x}_-)]/4$ . By Fourier transforming  $s_j(\mathbf{q}, t)$  we find

$$\begin{aligned} s_z(\mathbf{r}, t) &= \frac{1}{4} \left( e^{-\omega_+(q_{x_+}^a, 0)t} + e^{-\omega_-(q_{x_+}^a, 0)t} + 2e^{-\omega_+(0, q_{x_+}^a)t} \right) \cos(q_{x_+}^a x_+) \\ &\quad + \frac{1}{4} \left( e^{-\omega_+(q_{x_-}^b, 0)t} + e^{-\omega_-(q_{x_-}^b, 0)t} + 2e^{-\omega_+(0, q_{x_-}^b)t} \right) \cos(q_{x_-}^b x_-) \\ s_{x_+}(\mathbf{r}, t) &= \frac{1}{4} \left( e^{-\omega_+(q_{x_+}^a, 0)t} - e^{-\omega_-(q_{x_+}^a, 0)t} \right) \sin(q_{x_+}^a x_+), \end{aligned} \quad (10)$$

$$s_{x_-}(\mathbf{r}, t) = \frac{1}{4} \left( -e^{-\omega_+(q_{x_-}^b, 0)t} + e^{-\omega_-(q_{x_-}^b, 0)t} \right) \sin(q_{x_-}^b x_-). \quad (11)$$

Equations (9)–(11) show that the spin density excitation created initially with arbitrary wave vectors  $\mathbf{q}^a = q_{x_+}^a \hat{x}_+$  and  $\mathbf{q}^b = q_{x_-}^b \hat{x}_-$  will fully decay to zero as  $t \rightarrow \infty$ . While  $s_z(\mathbf{r}, t)$  decays with six distinct time constants,  $s_{x_+}(\mathbf{r}, t)$  and  $s_{x_-}(\mathbf{r}, t)$  decay with two time constants each. Interestingly, for  $\mathbf{q}^a = \mathbf{Q}_1 = Q_1 \hat{x}_+$ ,  $Q_1 = 4m^* \alpha_1 / \hbar^2$  and  $\alpha_1 = \beta_1$ , and  $\mathbf{q}^b = \mathbf{Q}_2 = Q_2 \hat{x}_-$ ,  $Q_2 = 4m^* \alpha_2 / \hbar^2$  and  $\alpha_2 = -\beta_2$ , we have  $\omega_-(Q_1, 0) = \omega_-(Q_2, 0) = 0$  and hence

$$s_z(\mathbf{r}, t \rightarrow \infty) = \frac{1}{4} [\cos(Q_1 x_+) + \cos(Q_2 x_-)], \quad (12)$$

$$s_{x_+}(\mathbf{r}, t \rightarrow \infty) = -\frac{1}{4} \sin(Q_1 x_+), \quad (13)$$

$$s_{x_-}(\mathbf{r}, t \rightarrow \infty) = \frac{1}{4} \sin(Q_2 x_-). \quad (14)$$

Equations (12)–(14) describe a PSL (crossed PSHs) within the diffusive approach [cf. Eq. (6)].

*Emerging PSL from a uniform spin polarization.* — A PSL pattern can also evolve from a uniform spin density, e.g.,  $s_z(\mathbf{r}, 0) = 1$  and  $s_{x_\pm}(\mathbf{r}, 0) = 0$ , as shown by Walser *et al.* [13] via time-resolved Kerr rotation microscopy. In this case the initial spin density contains all Fourier components

$$\begin{aligned} s_z(\mathbf{r}, t) &= \int [A_+(\mathbf{q})e^{-\omega_+(\mathbf{q})t} + A_-(\mathbf{q})e^{-\omega_-(\mathbf{q})t}] \cos(\mathbf{q} \cdot \mathbf{r}) d\mathbf{q} \\ s_{x_\pm}(\mathbf{r}, t) &= \int [\pm B_+(\mathbf{q})e^{-\omega_+(\mathbf{q})t} \mp B_-(\mathbf{q})e^{-\omega_-(\mathbf{q})t}] \sin(\mathbf{q} \cdot \mathbf{r}) d\mathbf{q} \end{aligned} \quad (15)$$

with  $A_{\pm}(\mathbf{q})$  and  $B_{\pm}(\mathbf{q})$  set by the initial conditions. Equations (15) and (16) show that all Fourier components of  $\mathbf{s}(\mathbf{r}, t)$  decay with time (cf. Eqs. (9)–(11), except those with the two ‘‘magic’’  $\mathbf{q}$ ’s:  $\mathbf{q}_1 = Q_1 \hat{x}_+$  and  $\mathbf{q}_2 = Q_2 \hat{x}_-$ . Hence for  $t \rightarrow \infty$  a PSL pattern emerges and could, in principle, be imaged with exactly the same experimental setup as in Ref. [13].

*Band anticrossing & spin texture.*— To see explicitly how the interband couplings  $\eta$  and  $\Gamma$  lead to unusual spin textures near the anticrossing [Fig. 2(a)], let us first write the Hamiltonian (2) in the decoupled ( $\eta = \Gamma = 0$ ) basis  $\{|\mathbf{k}, \nu, \pm\rangle\}$  [31]

$$\mathcal{H} = \begin{pmatrix} E_{1,\mathbf{k}}^+ & 0 & d_- & d_+ \\ 0 & E_{1,\mathbf{k}}^- & -d_+ & -d_- \\ d_-^* & -d_+^* & E_{2,\mathbf{k}}^+ & 0 \\ d_+^* & -d_-^* & 0 & E_{2,\mathbf{k}}^- \end{pmatrix}, \quad (17)$$

where  $E_{\nu,\mathbf{k}}^{\pm} = \varepsilon_{\nu,\mathbf{k}} \pm \Delta\varepsilon_s$  are the usual  $\nu^{\text{th}}$  Rashba-Dresselhaus bands [10],  $\Delta\varepsilon_s = k \sqrt{\alpha_v^2 + \beta_v^2 + 2\alpha_v\beta_v \cos 2\theta}$ , and

$$d_{\pm} = i \frac{k}{2} \left[ \eta \left( e^{-i(\phi_1 + \theta)} \pm e^{i(\phi_2 + \theta)} \right) - \gamma \left( e^{-i(\phi_1 - \theta)} \pm e^{i(\phi_2 - \theta)} \right) \right], \quad (18)$$

with  $e^{\pm i\phi_\nu} = [(\alpha_\nu - \beta_\nu) \sin \theta \pm i(\alpha_\nu + \beta_\nu) \cos \theta] k / \Delta\varepsilon_s$  and  $e^{\pm i\theta} = \cos \theta \pm i \sin \theta$ . The Hamiltonian in (17) shows that  $d_{\pm}$  (proportional to  $\eta$  and  $\Gamma$ ) couple  $E_{\nu,\mathbf{k}}^{\pm}$  with distinct ‘spin’ and orbital quantum numbers, thus leading to new dispersions  $E_{\mathbf{k},\lambda_1,\lambda_2}$  ( $\lambda_1, \lambda_2 = \pm 1$ ) that display anticrossings, Fig. 2(a), and spin mixing, Figs. 2(b) and 2(c) [32]. We can find the eigen-solutions of Eq. (17). These are too cumbersome to be shown here; a simple analytical case is presented in [33].

In what follows, we consider a realistic 530 Å InSb/Al<sub>0.4</sub>In<sub>0.6</sub>Sb double well of depth  $V_w = 613.3$  meV with a 360 Å Al<sub>0.12</sub>In<sub>0.88</sub>Sb central barrier of height  $V_b = 172.3$  meV. The total electron density is  $6.0 \times 10^{11}$  cm<sup>-2</sup> and arises from doping layers symmetrically placed 600 Å away from the center of the well. InSb wells have much larger SO strengths (cf. GaAs). For instance at  $V_g = 11$  meV, we obtain:  $\alpha_1 = 98$  meV Å,  $\alpha_2 = -90$  meV Å,  $\beta_1 = 50$  meV Å,  $\beta_2 = 51$  meV Å,  $\Gamma = -20$  meV Å, and  $\eta = -35$  meV Å, which are used in Figs. 2 and 3 [34].

Figure 2(a) shows the dispersions  $E_{\mathbf{k},-1,\lambda_2}$  (first subband) and  $E_{\mathbf{k},+1,\lambda_2}$  (second subband) for realistic InSb double well along the  $k_{x_+} = k_{x_-}$  direction. Note the anticrossing between  $E_{\mathbf{k},-1,+1}$  and  $E_{\mathbf{k},+1,-1}$  (dashed lines) around  $k_c$  [32, 35]. Figures 2(b) and 2(c) show the expectation values of the spin operators  $\sigma_x$  and  $\sigma_y$ , respectively. We can clearly see a strong spin mixing in  $\langle \sigma_x \rangle$  when the bands anticross. This follows from the interplay between the Rashba and Dresselhaus SO interactions. When only one of them is present, no spin mixing occurs, since in this case only same-spin branches couple.

Figure 3 shows the spin textures along constant-energy contours  $E_{\mathbf{k},\lambda_1,\lambda_2} = E_F, E'_F$  [short-dashed horizontal lines in Fig. 2(a)] due to the intersband SO-induced spin mixing. Figures 3(a)–3(b) and 3(c)–3(d) correspond to the cases in the presence and absence, respectively, of the interband SO couplings  $\eta$  and  $\Gamma$ . The arrows along the contours indicate the spin vector field  $\langle \sigma \rangle$  in the  $xy$  plane. The inner and outermost

contours (solids lines) in 3(a)–3(b) have spin textures consistent with the usual (uncoupled) Rashba-Dresselhaus shown in 3(c)–3(d). The dashed contours in 3(a)–3(b), on the other hand, show very distinctive spin textures below and above the crossing as compared to the uncoupled case.

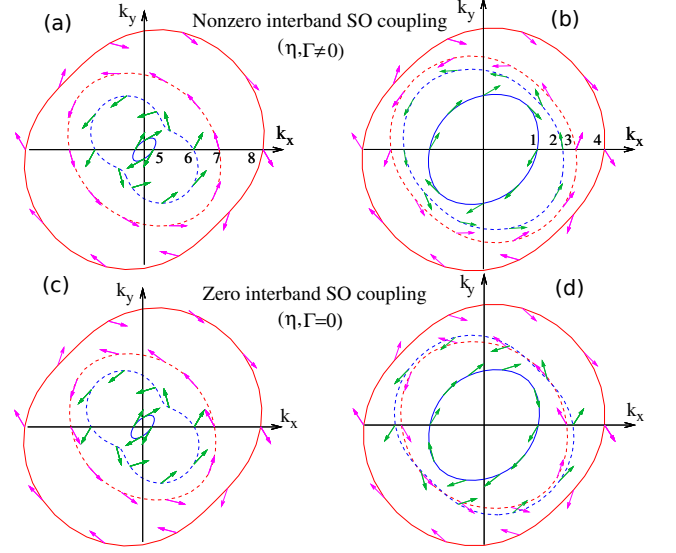


Figure 3. (Color online) Constant-energy contours and spin textures at  $E = E_F$  (a) and  $E = E'_F$  (b) in the presence of interband SO coupling. (c) and (d) show the case in the absence of  $\eta$  and  $\Gamma$  (usual Rashba-Dresselhaus bands). The arrows represent  $\langle \sigma \rangle$  along the contours below and above the anticrossing in Fig. 2(a).

*Spin relaxation mechanisms.*— In our (001)-grown GaAs well, the possible detrimental factors leading to the decay of the PSL are the D’yakonov-Perel (DP) spin relaxation mechanism, due to the cubic Dresselhaus term [11, 12, 36], and an Elliott-Yafet (EY)-type mechanism, due to the interband coupling [37]. The DP time for each subband is given by  $\tau_v^{DP} = 4\hbar^2 / (\gamma^2 k_{F,v}^6 \tau)$  [38]. To evaluate the induced-interband coupling EY relaxation time, we follow Ref. 37 and obtain  $\tau_v^{EY} \sim (\Delta E / \eta k_{F,v})^2 \tau_{IB}$ , in which  $\Delta E$  is the energy difference between subbands 1 and 2, and  $\tau_{IB}$  the interband scattering time [39]. For our GaAs well, with  $\gamma \sim 11.0$  eV Å<sup>3</sup> [21, 40],  $k_{F,v} \sim 0.01$  Å<sup>-1</sup>, and  $\tau, \tau_{IB} \sim 1$  ps [41], we find  $\tau_v^{DP} \sim 15$  ns [42] and  $\tau_v^{EY} \sim 10$  ns. These estimates for  $\tau_v^{DP}$  and  $\tau_v^{EY}$  suggest that our PSL can be experimentally detected [43].

*Concluding remarks.*— We have performed a self-consistent calculation in double wells with two occupied subbands to determine all SO couplings. We find a unique configuration with  $\alpha_1 = \beta_1$  and  $\alpha_2 = -\beta_2$  (and  $\beta_1 \approx \beta_2$ ), which allows for a Persistent Skyrmion Lattice in the non-interacting 2D electron gas away from anti crossings. The interband coupling  $\eta$  plays a role comparable to that of the cubic Dresselhaus term in limiting the lifetime of the PSL. For  $E_F$  near anticrossings, we find a strong spin mixing between different band branches and no PSL. We conjecture that a PSL formed on top of an electrically drifting Fermi sea [45] can possibly lead to a ‘topological Hall effect’ [17] in ordinary GaAs wells.

We thank R. Raimondi, R. Winkler, A. Vishwanath and J. Fabian for useful discussions. This work was supported by FAPESP, CNPq, PRP/USP (Q-Nano), the Swiss NSF, NCCR QSIT, and the Natural Science Foundation of China (Grant No. 11004120).

\* Permanent address: Department of Physics, Qufu Normal University, Qufu, Shandong, 273165, China.

- [1] C. L. Kane, and E. J. Mele, *Phys. Rev. Lett.* **95**, 146802 (2005).
- [2] B. A. Bernevig, T. L. Hughes, and S. C. Zhang, *Science* **314**, 1757 (2006).
- [3] M. König, S. Wiedmann, C. Brüne, A. Roth, H. Buhmann, L. W. Molenkamp, X.-L. Qi, and S. C. Zhang, *Science* **318**, 766 (2007).
- [4] O. Pankratov, S. Pakhomov, and B. Volkov, *Solid State Commun.* **61**, 93 (1987).
- [5] J. Alicea, *Rep. Prog. Phys.* **75**, 076501 (2012).
- [6] S. L. Sondhi, A. Karlhede, S. A. Kivelson, and E. H. Rezayi, *Phys. Rev. B* **47**, 16419 (1993).
- [7] L. Brey, H. A. Fertig, R. Côté, and A. H. MacDonald, *Phys. Rev. Lett.* **75**, 2562 (1995).
- [8] S. Mühlbauer *et al.* *Science* **323**, 915 (2009); X. Z. Yu *et al.* *Nature* **465**, 901 (2010); S. Seki *et al.* *Science* **336**, 198 (2012). See also M. B. A. Jalil and S. G. Tan, *Sci. Rep.* **4**, 5123 (2014).
- [9] A. W. Overhauser, *Phys. Rev.* **128**, 1437 (1962).
- [10] J. Schliemann, J. C. Egues, and D. Loss, *Phys. Rev. Lett.* **90**, 146801 (2003).
- [11] B. A. Bernevig, J. Orenstein, and S. C. Zhang, *Phys. Rev. Lett.* **97**, 236601, (2006).
- [12] J. D. Koralek, C. Weber, J. Orenstein, B. A. Bernevig, S. C. Zhang, S. Mack, and D. Awschalom, *Nature* **458**, 610 (2009).
- [13] M. P. Walsler, C. Reichl, W. Wegscheider, and G. Salis, *Nature Physics* **8**, 757 (2012).
- [14] The PSH symmetry point is also investigated by Sasaki *et al.*, *Nat. Nanotechnol.* **9**, 703 (2014).
- [15] E. Bernardes, J. Schliemann, M. Lee, J. C. Egues, and D. Loss, *Phys. Rev. Lett.* **99**, 076603 (2007).
- [16] S. Souma, H. Mukai, M. Ogawa, A. Sawada, S. Yokota, Y. Sekine, M. Eto, T. Koga, arXiv:1304.6992.
- [17] B. Binz and A. Vishwanath, *Physica B* **403**, 1336 (2008).
- [18] R. Raimondi, C. Gorini, P. Schwab, and M. Dzierzawa, *Phys. Rev. B* **74**, 035340 (2006).
- [19] X. Liu and J. Sinova, *Phys. Rev. B* **86**, 174301 (2012).
- [20] R. Winkler, *Spin-Orbit Coupling Effects in Two-Dimensional Electron and Hole Systems*, *Springer Tracts in Modern Physics* Vol. 191 (Springer, New York, 2003).
- [21] F. Dettwiler, J. Y. Fu, P. J. Weigele, S. Mack, J. C. Egues, D. D. Awschalom, and D. Zumbühl, arXiv:1403.3518.
- [22] R. S. Calsaverini, E. Bernardes, J. C. Egues, and D. Loss, *Phys. Rev. B* **78**, 155313 (2008).
- [23] S. V. Iordanskii, Y. B. Lyanda-Geller, and G. E. Pikus, *JETP Lett.* **60**, 199 (1994).
- [24] The matrix elements  $\eta$  and  $\Gamma$  can be chosen real, see footnote [15] in Ref. [15].
- [25] We assume  $V(\mathbf{r})$  is the same for both subbands.
- [26] We take  $\varphi(\mathbf{r})$  as a constant here. In the case of a weak disorder potential, it should resemble a plane wave.
- [27] J. Fabian and M. W. Wu, *Handbook of Spin Transport and Magnetism* (CRC Press, Florida, 2012), p. 312.
- [28] E. G. Mishchenko, A. V. Shytov, and B. I. Halperin, *Phys. Rev. Lett.* **93**, 226602 (2004).
- [29] A. A. Burkov, A. S. Núñez, and A. H. MacDonald, *Phys. Rev. B* **70**, 155308 (2004).
- [30] M. Duckheim, D.L. Maslov, and D. Loss, *Phys. Rev. B* **80**, 235327 (2009).
- [31] Here  $\langle \mathbf{r} | \mathbf{k}, \nu, \pm \rangle = e^{i\mathbf{k}\cdot\mathbf{r}} (1, \pm e^{i\varphi_\nu(\mathbf{k})})^T / \sqrt{2}$ ,  $\varphi_\nu(\mathbf{k}) = \arg[(\alpha_\nu - \beta_\nu)k_{x_-} + i(\alpha_\nu + \beta_\nu)k_{x_+}]$ .
- [32] Some of these features resemble the data of Bentmann *et al* [*Phys. Rev. Lett.* **108**, 196801 (2012)].
- [33] Interestingly, for  $\alpha_1 = \beta_1$ ,  $\alpha_2 = \beta_2$  and  $\eta = -\Gamma$ , we have  $E_{\mathbf{k},\nu}^\pm = \varepsilon_{\mathbf{k},\nu} \pm 2\alpha_\nu |k_{x_\pm}|$ ,  $d_+ = -2i\eta k_{x_+} k_{x_-} / |k_{x_\pm}|$ , and  $d_- = 0$ . The Hamiltonian in Eq. (17) then decouples into two subspaces  $\mathcal{F}_\pm = \{|\mathbf{k}, 1, \pm\rangle, |\mathbf{k}, 2, \mp\rangle\}$  with eigensolutions 
$$E_{\mathbf{k},\lambda_1,\lambda_2} = \varepsilon_{\mathbf{k},+} + \lambda_1 \lambda_2 2\alpha_- |k_{x_+}| + \lambda_1 \sqrt{(\varepsilon_{\mathbf{k},-} + \lambda_1 \lambda_2 2\alpha_+ |k_{x_+}|)^2 + 4\eta^2 k_{x_-}^2}, \quad (19)$$
$$|\mathbf{k}, \lambda_1, \lambda_2\rangle = \sum_{\nu=1}^2 \left[ \cos\left(\frac{\varphi}{2}\right) \frac{1 + (-1)^\nu \lambda_1}{2} |\mathbf{k}, \nu, \text{sgn}(\lambda_2)\rangle + i\lambda_1 \lambda_2 \frac{k_{x_+}}{|k_{x_+}|} \sin\left(\frac{\varphi}{2}\right) \frac{1 - (-1)^\nu \lambda_1}{2} |\mathbf{k}, \nu, -\text{sgn}(\lambda_2)\rangle \right], \quad (20)$$
where  $\varepsilon_{\mathbf{k},\pm} = (\varepsilon_{2,\mathbf{k}} \pm \varepsilon_{1,\mathbf{k}})/2$ ,  $\alpha_\pm = (\alpha_2 \pm \alpha_1)/2$ ,  $\tan \varphi = 2\eta k_{x_-} / \Delta\varepsilon$ , and  $\Delta\varepsilon = \varepsilon_{\mathbf{k},-} + \lambda_1 \lambda_2 2\alpha_+ |k_{x_+}|$ . The quantum numbers  $\lambda_1$  and  $\lambda_2$  index the eigensolutions and can take the values  $\pm 1$ .
- [34] To enhance the anticrossings and spin textures in Figs. 2 and 3, we have scaled up the SO couplings by a factor of 10.
- [35] For  $\theta = \pi/4$ , which corresponds to the direction  $k_{x_+} = k_{x_-}$ , we have  $k_c = (\varepsilon_2 - \varepsilon_1) / [(\alpha_1^2 + \beta_1^2)^{1/2} + (\alpha_2^2 + \beta_2^2)^{1/2}]$ .
- [36] M. C. Lüffe, J. Kailasvuori, and T. S. Nunner, *Phys. Rev. B* **84**, 075326 (2011).
- [37] S. Döhrmann, D. Hägele, J. Rudolph, M. Bichler, D. Schuh, and M. Oestreich, *Phys. Rev. Lett.* **93**, 147405 (2004).
- [38] F. Meier and B.P. Zakharchenya, *Optical Orientation* (North-Holland, Amsterdam, 1984).
- [39] To estimate  $\tau_v^{EY}$ , we apply perturbation theory to Hamiltonian (2) with  $\alpha_\nu = \beta_\nu = 0$ . The first-order renormalized states for each subband are given by  $|\mathbf{k}, \nu, \uparrow\rangle^{(1)} = |\mathbf{k}, \nu, \uparrow\rangle - (-1)^\nu a^*(\mathbf{k}) |\mathbf{k}, \nu', \downarrow\rangle$  and  $|\mathbf{k}, \nu, \downarrow\rangle^{(1)} = |\mathbf{k}, \nu, \downarrow\rangle - (-1)^\nu a(\mathbf{k}) |\mathbf{k}, \nu', \uparrow\rangle$ , respectively, with  $a(\mathbf{k}) = (i\eta k_- + \Gamma k_+) / \Delta E$ ,  $k_\pm = k_x \pm ik_y$  and  $\Delta E$  the energy difference between subbands 1 and 2. We then have  $\tau_v^{EY}(\mathbf{k})^{-1} \sim 2\pi \sum_{\mathbf{k}'}$   $|^{(1)}\langle \mathbf{k}', 1, \downarrow | V(\mathbf{r}) | \mathbf{k}, 1, \uparrow \rangle|^{(1)2} \delta(E_{\mathbf{k}'} - E_{\mathbf{k}})$ , with  $V(\mathbf{r})$  the scattering potential. A straightforward calculation yields  $\tau_v^{EY} \sim (\Delta E / \eta k_{F,\nu})^2 \tau_{IB}$ . Here we neglect the terms proportional to  $\Gamma$  ( $\eta \gg \Gamma$ ). We assume  $\tau_{IB} \sim \tau$ . Note that our perturbation theory ( $\eta k / \Delta E \ll 1$ ) is only valid far below  $k_c$ , i.e.  $k \ll \Delta E / \eta \sim k_c$  ( $\alpha_\nu$  and  $\eta$  comparable).
- [40] J. Y. Fu and J. Carlos Egues, *Phys. Rev. B* **91**, 075408 (2015).
- [41] R. Raimondi and P. Schwab, *Physica E* **42**, 952 (2010).
- [42] Since we are calculating the relaxation time away from  $k_c$  (see Ref. [39]), we have neglected the contribution of the interband couplings to the cubic Dresselhaus, which in this case would read  $\beta_{3,\nu}^\pm = \beta_{3,\nu} + k^2 [\beta_\nu \eta^2 \mp \alpha_\nu \Gamma^2 - \eta \Gamma (\alpha_\nu \mp \beta_\nu)] / \Delta E^2$ , up to  $\mathcal{O}(\Delta E^{-2})$ .
- [43] We have neglected the effect of the random Rashba on the decaying of our crossed PSHs. This effect is tiny in GaAs wells [40, 44].
- [44] E. Ya. Sherman, *Appl. Phys. Lett.* **82**, 209 (2003).
- [45] L. Yang, J. D. Koralek, J. Orenstein, D. R. Tibbetts, J. L. Reno and M. P. Lilly, *Nat. Phys.* **8**, 153 (2012).